

# Parallel Polar Dimers in the Columnar Self-Assembly of Umbrella-Shaped Subphthalocyanine Mesogens

Matthias Lehmann,\* Maximilian Baumann, Martin Lambov, and Alexey Eremin\*

In memory of Professor Siegfried Hünig

The self-assembly of umbrella-shaped mesogens is explored with subphthalocyanine cores and oligo(thienyl) arms with different lengths in the light of their application as light-harvesting and photoconducting materials. While the shortest arm derivatives self-assemble in a conventional columnar phase with a single mesogen as a repeating unit, the more extended derivatives generate dimers that pile up into liquid crystalline columns. In contrast to the antiparallel arrangement known from single crystals, the present mesogens align as parallel dimers in polar columnar phases as confirmed by X-ray scattering, experimental densities, dielectric spectroscopy, second harmonic generation, alignment, and conductivity studies. UV-vis and fluorescence spectroscopies reveal a broad absorption in the visible range and only weak emission of the Q-band. Thus, these light-collecting molecules forming strongly polar columnar mesophases are attractive for application in the area of photoconductive materials.

non-chiral bent-shaped mesogens,<sup>[4]</sup> supra-molecular mesogens,<sup>[5]</sup> flexible bowl-shaped cyclophanes,<sup>[6,7]</sup> chiral discotics<sup>[8–10]</sup> and to shape-persistent, concave subphthalocyanines (SubPc).<sup>[11–14]</sup> The latter possess a central boron atom with an axial substituent X (X = halogen, alkoxy or aryloxy). They are rigid bowls with large permanent dipole moments along the B-X axis, and reveal considerable absorption coefficients in the visible range of their spectra.<sup>[15]</sup> Therefore, crystalline and LC derivatives of SubPcs were studied as non-linear optical materials,<sup>[11]</sup> as acceptor molecules for photovoltaic cells,<sup>[16]</sup> and pyroelectric and ferroelectric materials.<sup>[12,17]</sup> Recently, polar phases were demonstrated to reveal an anomalous or bulk photovoltaic effect, i.e., a

photo current without any p-n junction, in SmC\* phases of semi-conducting calamitics and columnar phases of SubPcs.<sup>[18–20]</sup> This behavior is especially interesting, since in most organic materials the low dielectric constant hampers the charge generation and separation owing to the strong coulomb interaction of the ion pairs. Polar properties also lead to the recent success of inorganic materials for applications in photovoltaic devices.<sup>[21]</sup> Obviously, the polarity of the phase assists charge separation. In addition, the bowl shape and axial substituent lower the clearing temperatures compared to the related phthalocyanine mesogens.<sup>[22]</sup> The polar phase structure enables the complete and facile homeotropic alignment by the application of a DC field.<sup>[12,20]</sup> These are two preconditions which have to be fulfilled in columnar LC phases, when an application in organic photovoltaics is envisioned.

In the present study, we designed a new star mesogen by combining the SubPc core with fluorine as the smallest axial substituent with three shape-persistent arms (**Figure 1**). It was recently found, that intrinsic free space generated between such arms drives the self-assembly of star mesogens into dimers stacked in a helical fashion.<sup>[22,23]</sup> Upon irradiation, the absorbed photon energy is transferred to the core and consequently the conjugated arms may serve as antennas for the collection of light.<sup>[22,24]</sup> Here, we demonstrate that the new mesogens **1a–c** assemble in low clearing-temperature columnar LC phases with an absorption over a large part of the visible spectral range. X-ray scattering (XRS), polarized optical microscopy (POM), differential scanning calorimetry (DSC) and density studies clearly show that the smallest more conventional mesogen **1a** stacks in columns, in which a single molecule is the repeating unit, while the star-like umbrella-shaped mesogens **1b,c** form enantiotropic LC phases


## 1. Introduction

Since their discovery in 1975, polar liquid crystals (LCs) of chiral, rod-shaped mesogens became a fundamental research topic.<sup>[1]</sup> Owing to the richness of structures, such as various ferro-, ferri-, pyro- or antiferroelectric states, polar LCs found broad applications in waveguides, switches, modulators or optical filters.<sup>[2,3]</sup> Since then, the field has been expanded to polar phases from

Prof. M. Lehmann, M. Baumann, M. Lambov  
Institute of Organic Chemistry  
University of Würzburg  
97074 Würzburg, Germany  
E-mail: matthias.lehmann@uni-wuerzburg.de

Prof. M. Lehmann  
Center for Nanosystems Chemistry and Bavarian Polymer Institute  
University of Würzburg  
97074 Würzburg, Germany

Prof. A. Eremin  
Institute of Physics  
Otto von Guericke University  
39106 Magdeburg, Germany  
E-mail: alexey.eremin@ovgu.de

 The ORCID identification number(s) for the author(s) of this article can be found under <https://doi.org/10.1002/adfm.202104217>.

© 2021 The Authors. Advanced Functional Materials published by Wiley-VCH GmbH. This is an open access article under the terms of the Creative Commons Attribution-NonCommercial License, which permits use, distribution and reproduction in any medium, provided the original work is properly cited and is not used for commercial purposes.

DOI: 10.1002/adfm.202104217

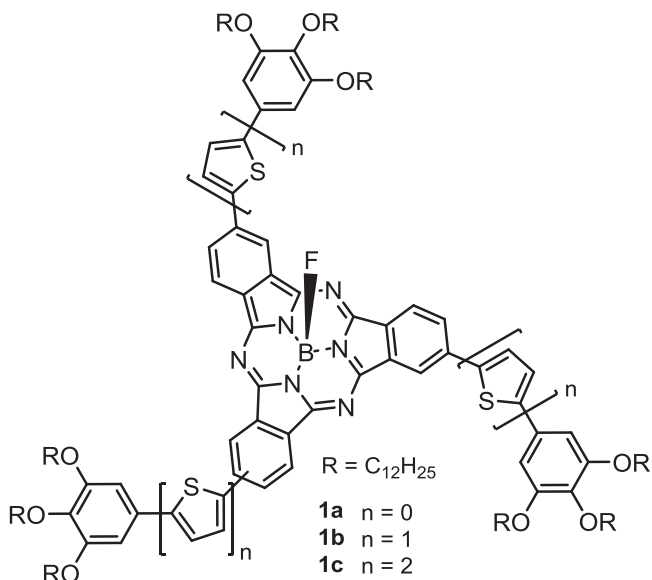


**Figure 1.** Umbrella-shaped SubPc target structures **1a–c**.

with low clearing temperatures (<200 °C) consisting of columns, in which dimers with parallel dipoles assemble as smallest columnar building blocks. These star-shaped SubPcs arrange in polar columnar LCs as evidenced by second-harmonic generation and can be homeotropically aligned in an electric field.

## 2. Synthesis

In a convergent synthesis, the arm components **3**, **4**, and **5**, which were functionalized with boronic acids or boronic acid esters, were joint via a threefold Suzuki cross coupling with the triiodosubphthalocyaninefluoride **2** (**Figure 2A**).<sup>[12,25]</sup> This resulted in 25–53% of the target compounds after a thorough purification with a final recycling GPC separation. The mixture of C<sub>1</sub>/C<sub>3</sub> diastereomers of the triodo SubPcs in the statistical ratio of 3:1 was confirmed by NMR spectroscopy (**Figure 2B**). It had not been separated prior to the final coupling step and consequently the expected statistic mixture of isomers was found also in the final products.<sup>[25,26]</sup> We anticipated this to result in the desired low transition temperatures for the LC materials. The purity and identity were confirmed by standard NMR spectroscopy and high-resolution mass spectrometry (see experimental part and Supporting Information).

## 3. Optical Properties

**Figure 3** highlights the absorption and emission spectra of the target compounds. The increase of the conjugated system from the molecule with the 3,4,5-dodecyloxy phenyl arm to the derivative with the 3,4,5-dodecyloxyphenyldithienyl arm shifts the Soret and the Q-bands bathochromically from 364 nm, 584 nm (**1a**) to 404 nm, 604 nm (**1b**) and 430 nm, 612 nm (**1c**). The maxima at 280, 330, and 367 nm for **1a–c** are attributed to the absorption of the conjugated arms. The extinction coefficient for the bathochromically shifted Q-bands of **1b** and **1c** is approximately by a factor of two higher compared with **1a**. This can be attributed to a lower

twisting angle between SubPc core and arm and consequently an increased conjugation when a thienyl group joins the core with the peripheral unit (**Figure 4** and Supporting Information).

The thin film absorption (**Figure 3B**) exhibits a typical broadening of the spectra. Especially compounds with large conjugated arms display a strong absorption over a broad band in the visible range from 400 to 700 nm. This is analogous with the increase in absorption for non-LC star-shaped porphyrins, which are advantageously applied in photovoltaic cells.<sup>[27]</sup> Temperature-dependent absorption spectroscopy of LC films reveals an increase in the short wavelength vibrational band of the Q-band when cooling from the isotropic to the LC state, indicating the formation of columnar stacks (**Figure 3B** and **Figure S19**, Supporting Information). All compounds show an orange-red emission when excited by UV-light (380–420 nm) in CH<sub>2</sub>Cl<sub>2</sub> solution (**Figure 3D** and **Figure S20**, Supporting Information). **Figure 3C** highlights a concentration corrected fluorescence study. It demonstrates that for irradiation in bands of similar extinction coefficient  $\lambda_{\text{ex}}$  (1) = 280 nm (**1a**) and  $\lambda_{\text{ex}}$  (4) = 404 nm (**1b**) or  $\lambda_{\text{ex}}$  (2) = 330 nm (**1b**) and  $\lambda_{\text{ex}}$  (3) = 367 nm (**1c**) the emission is most efficient for compound **1b**. Interestingly, when the solvent evaporates the emission is completely quenched for **1b** and **1c** in thin LC films, while for **1a** a residual very weak emission remains (**Figure S20**, Supporting Information). This can be explained by the weaker aggregation tendency of **1a** compared with **1b,c** owing to the naturally twisted conformation of peripheral phenyl groups and their steric repulsion along the columns.

## 4. Thermotropic Properties

The mesomorphic behavior has been studied by POM, DSC and variable temperature XRS.

POM (**Figure 5A–C**) reveals fluid materials with pseudo-focal conic and mosaic textures and homeotropic domains suggesting hexagonal columnar LC phases. In contrast to **1b** and **1c**, compound **1a** is a material with a comparatively low viscosity at ambient temperature. The clearing points at 79.5 °C (**1a**), 146.2 °C (**1b**) and 165.2 °C (**1c**) are significantly lower than the clearing temperatures of related phthalocyanines, which decompose without clearing at  $T > 300$  °C.<sup>[22]</sup> DSC cycles for **1a** and **1a** show broad transitions with small hystereses and low transition enthalpies at 79.5 °C ( $\Delta H = 4.1$  kJ mol<sup>-1</sup>, hysteresis 3.3 °C) and 165.2 °C ( $\Delta H = 1.4$  kJ mol<sup>-1</sup>, no hysteresis) pointing to materials with low degree of order. Compound **1b** exhibits a more defined first order transition at 146.2 °C ( $\Delta H = 5.1$  kJ mol<sup>-1</sup>) with a hysteresis of 3.3 °C (see Supporting Information). The broad transitions for **1a** and **1c** are presumably a consequence of the mixtures of diastereomers and the conformation of the arms. While **1a** possesses twisted peripheral units, the arms in **1b** and **1c** can be coplanar with the core (**Figure 4** and **Figure S22**: Supporting Information), but the latter may form a large number of planar conjugated conformers. For compounds **1b** and **1c** glass transitions at 74.7 and 103.0 °C are consistent with the increasing viscosity and absence of fluidity at low temperature.

The LC structures were elucidated by temperature variable wide-angle XRS on aligned (extruded) fibers and determination of the density by the buoyancy method. Extrusion from the LC phases (above 70 °C) resulted only in partial alignment for **1a**. The alignment could be improved by extrusion at lower

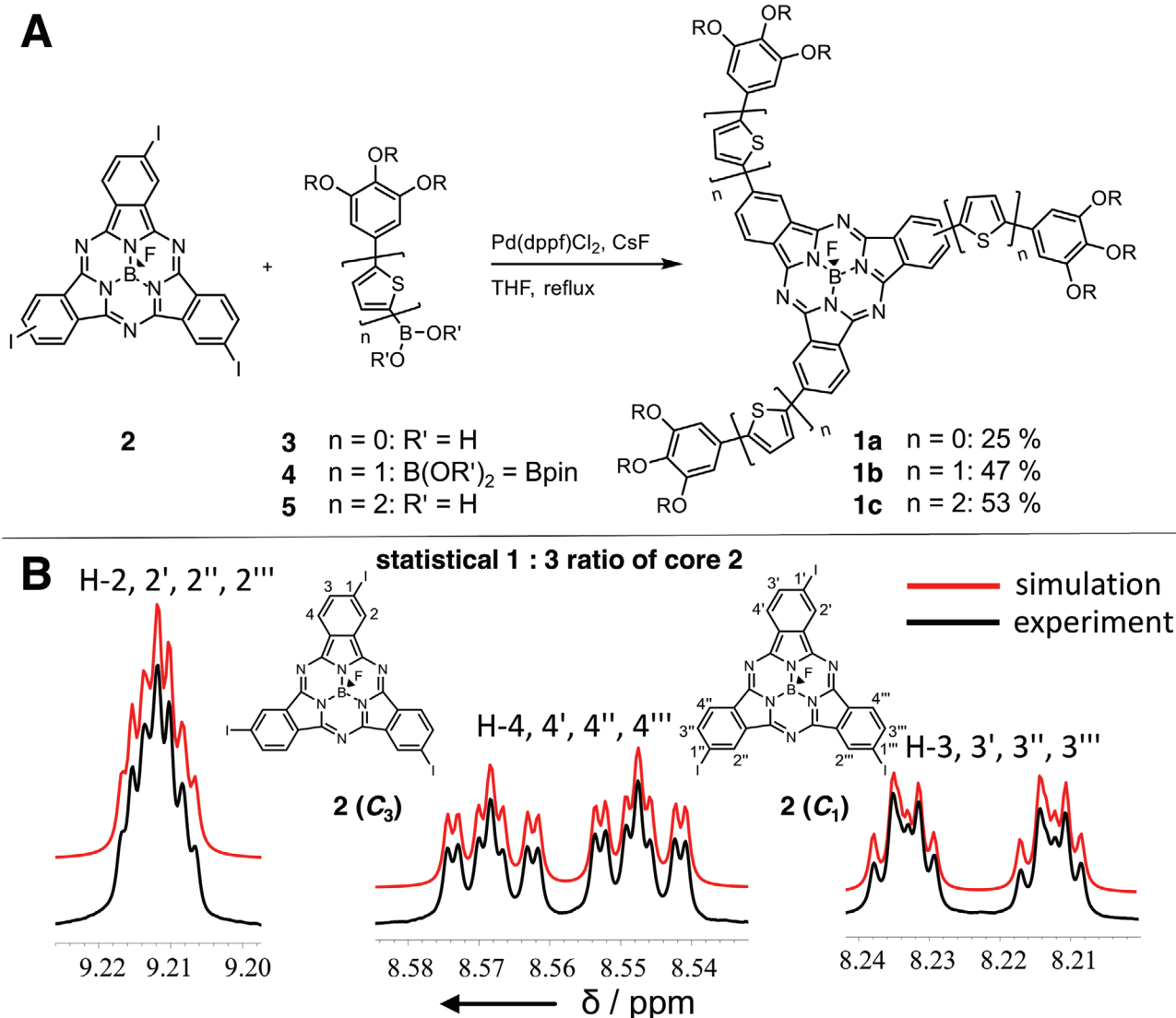


**Figure 2.** A) Convergent synthesis of the target structures **1a–c**. Bpin = boronic acid pinacol ester. B) Experimental and simulated NMR spectra of the core derivative **2**. The spectrum can be perfectly fitted as a mixture of diastereomers in a 1:3 ratio, which is the expected statistical ratio for the  $C_3$  and  $C_1$  symmetric diastereomers evolved from synthesis. The chemical shifts and coupling constants for the simulated spectra are given in the experimental part.

temperatures, close to RT, while for **1b** the alignment was best at 100 °C (see Supporting Information). The theta-scans along the equator and the meridian of the XRS patterns are shown in Figure 5D. The intensity profiles are consistent with hexagonal columnar phases for **1a** ( $a = 36.8$  Å, 50 °C), **1b** ( $a = 44.3$  Å, 25 °C) and **1c** ( $a = 51.1$  Å, 115 °C) owing to reflections of mixed indices (11, 21), although for **1b** they are extremely weak (Figure S14, Supporting Information). The diffuse scattering, which is assigned as halo, corresponds to the liquid-like order of the aliphatic chains. Only for **1c** a broad signal reveals at larger scattering angles and this is associated with  $\pi$ - $\pi$  distances of aromatic units. However, the correlation length is of short range typical for the next neighbor-order in liquids. Further diffuse scattering maxima are positioned at the meridian for **1a** corresponding to a liquid-like order with a mean distance of 7.6 Å along the column and at the equator, thus, orthogonal

to the column, for **1b** (9.5 Å) and **1c** (7.5 Å). These latter signals are related to some liquid-like intracolumnar nearest-neighbor correlations. The densities determined at 25 °C give more insights. They amount to 0.874 g cm<sup>-3</sup> (**1a**), 1.017 g cm<sup>-3</sup> (**1b**) and 1.019 g cm<sup>-3</sup> (**1c**). Thus at 50 °C, two mesogens **1a** fit in a columnar unit of 7.6 Å height (the estimated density at 50 °C is 0.862 g cm<sup>-3</sup>, see Supporting Information). Thus, the meridional diffuse signal can be explained only if two SubPcs are arranged in an axial fashion, but the arms are staggered to each other, owing to their out-of-plane arrangement. This is a rather conventional self-assembly as found by Torres and Araoka and in most single crystal structures.<sup>[15,20,28]</sup> The subsequent rather loose packing explains the low density, low viscosity, and the residual fluorescence in the solid state. Although the space between the arms in the derivatives **1b** and **1c** is increasing, the densities are increasing as well pointing to a

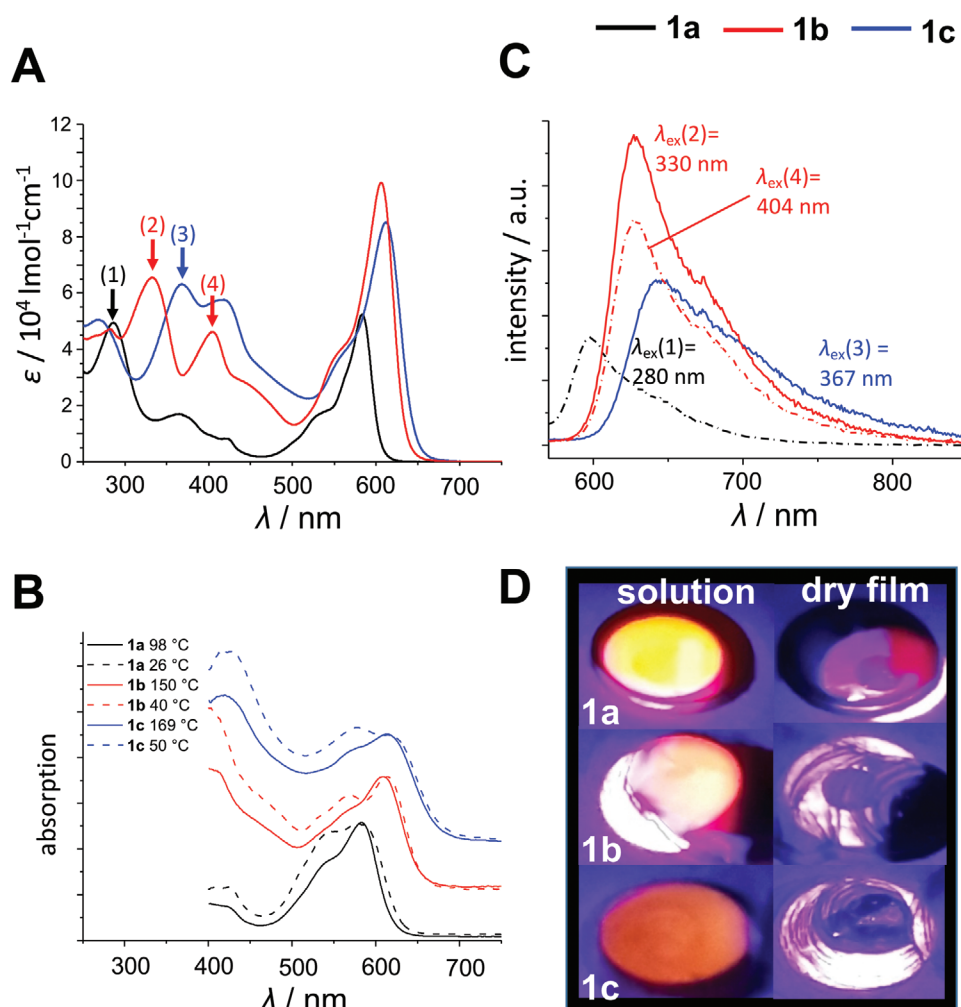


**Figure 3.** A) UV-Vis absorption in  $\text{CHCl}_3$ . B) UV-Vis absorption of thin films in the isotropic phase (dashed line) and the liquid crystal (solid line). C) Fluorescence spectra in  $\text{CHCl}_3$ . These spectra are recorded with identical instrumental parameters at similar concentrations ( $10^{-7} \text{ mol L}^{-1}$ ) and are concentration corrected in order to compare the relative fluorescence quantitatively. The arrows in (A) indicate the excitation wavelengths for (C). D) Fluorescence images of the compounds in solution ( $\text{CH}_2\text{Cl}_2$ , left) and as dry solid films (right);  $\lambda_{\text{ex}} = 380\text{--}420 \text{ nm}$ .

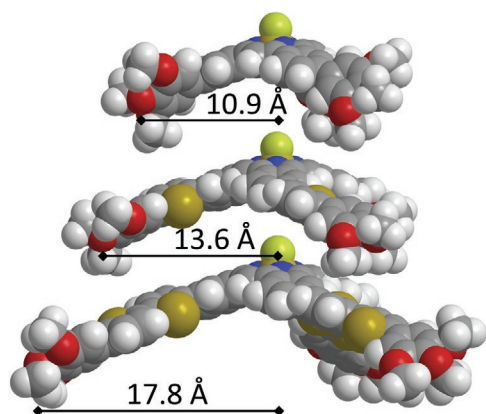


**Figure 4.** Radial extension of target structures **1a–c** from energy optimized models (see Supporting Information). The peripheral arm of the smallest molecule is twisted by  $36.8^\circ$  out of the aromatic plane of the core (cp. Figure S22, Supporting Information).

more compact aggregation. And indeed, the calculation of the numbers of mesogens in a columnar slice of  $4.9 \text{ \AA}$  (**1b**) or  $4.2 \text{ \AA}$  (**1c**) reveals that there are two mesogens. In that small height of the columnar slice these mesogens can only arrange side by side. These findings are also in agreement with the increase in columnar diameter from **1a** to **1b** ( $7.5 \text{ \AA}$ ), which is larger than expected when compared with the increase of the molecular diameters ( $5.0 \text{ \AA}$ ) of such bowl-shaped mesogens (see Figure 4 and Supporting Information). The dimer formation is analogous to other star mesogens, which frequently assemble in double helices to compensate the intrinsic free space between the arms.<sup>[23]</sup> The diffuse equatorial scattering is attributed to the intracolumnar distances between the single molecules of these dimers. Missing meridional reflections indicate that double helices are not formed in the present system. This might originate from the mixture of diastereomers, which does not assist the formation of such regular structures. However, for steric reasons there must be an angular mismatch between the nearest

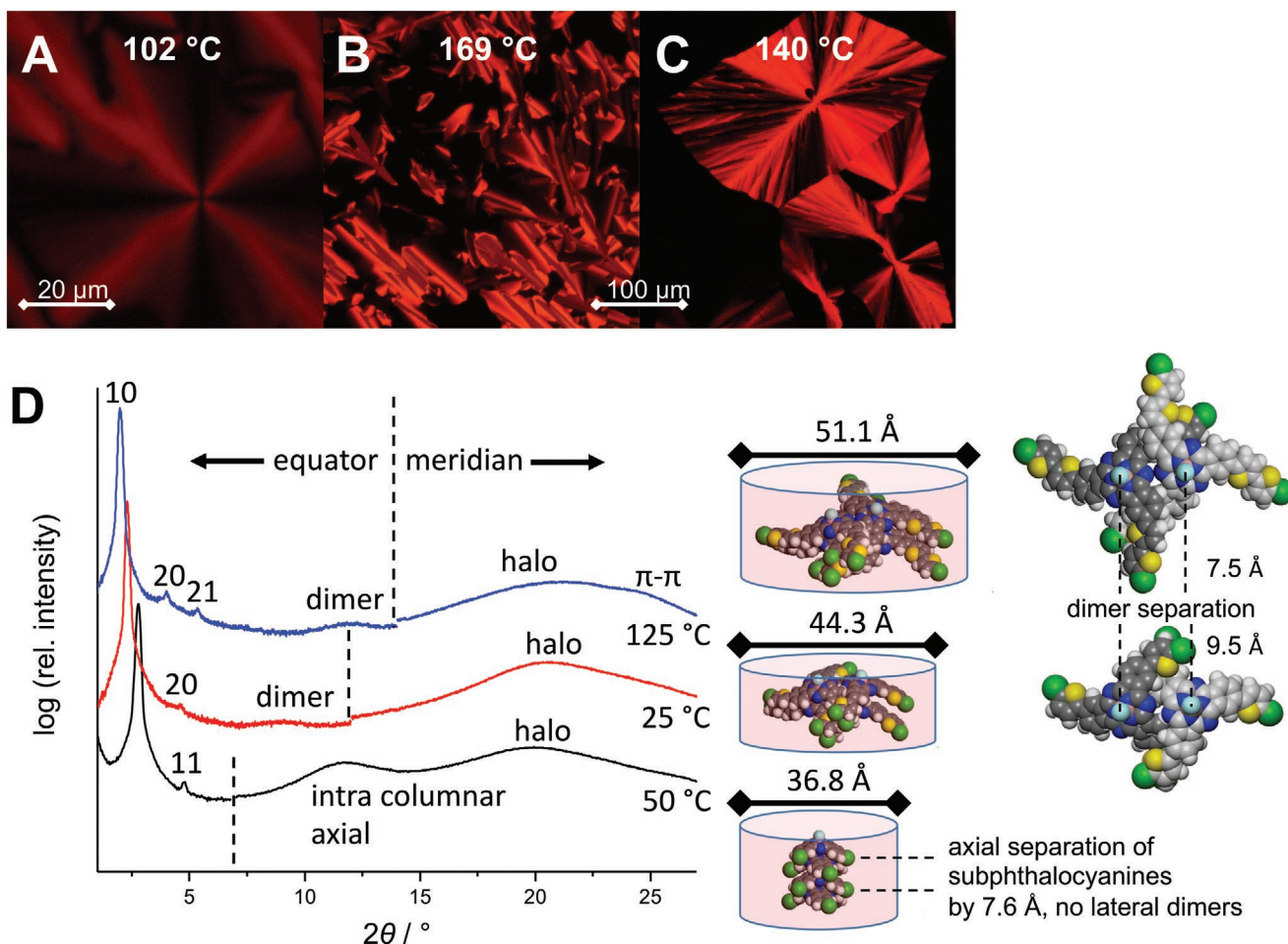


**Figure 5.** A–C) Characteristic POM textures of liquid crystals of **1a–c** between glass slides cooled from the isotropic phase with  $1\text{ }^{\circ}\text{C min}^{-1}$ . Pseudo-focal conic textures of **1a** at  $102\text{ }^{\circ}\text{C}$  (A) and **1b** at  $140\text{ }^{\circ}\text{C}$  (C). Mosaic texture of **1c** at  $169\text{ }^{\circ}\text{C}$  (B). D) Intensity profiles of temperature-dependent 2D X-ray patterns of compounds **1a** (black), **1b** (red) and **1c** (blue) along the equator and the meridian. Right: models of columnar stacks. For **1a** single mesogens stack along the column axis, while for **1b** and **1c** the stars form first dimers and subsequently stack in columns.

neighbors in the column. In almost all single crystal structures of SubPcs the bowl-shaped molecules pack antiparallel, which is driven by the reduction of the electrostatic dipole energy. Such antiparallel alignment causes a non-polar ground-state and consequently no second harmonic generation (SHG) is allowed. Indeed, this is the result of Torres and Araoka, when they investigated their LC samples without external applied electric field presumably owing to antiparallel columns.<sup>[12,20]</sup> In the presence of an E-field the macroscopic dipoles align parallel and large SHG signals were recorded. Similarly, the columnar phases of **1b** and **1c** exhibit strong SHG signals after cooling from the isotropic liquid to the LC phase in the DC field (Figure 7). This clearly demonstrates the presence of polar domains which can only be formed when the dimers in the individual columns are oriented parallel.

## 5. Structure Modelling

In order to rationalize these findings, we constructed a model of short columnar aggregates with the program

suite *Materials Studio*. Mesogen **1a** can be stacked like in a columnar phase of cone-shaped molecules and most crystalline SubPc structures.<sup>[6,7,15,28]</sup> The staggered orientation of the peripheral units accounts for the periodicity along the columns (Figure 6A). The larger SubPc stars generate propeller-shaped parallel dimers (Figure 6B). They were rotated by  $20^{\circ}$  about the column axis in order to avoid the steric repulsion. For the antiparallel dimer this rotation is not possible for steric reasons (Figure 6C). The subsequent geometry optimization leads in both cases to strongly negative non-bonding interactions (van der Waals and electrostatic interactions) indicating the stability of these possible supramolecular arrangements. While for the helical model with parallel dimers the building blocks (core and aliphatic chains) are nanosegregated in a central column and its periphery, in the antiparallel case, which is even lower in energy, all cores are coplanarly stacked and the aliphatic chains fill completely the intrinsic free space between the aromatic arms. Thus, this antiparallel structure resembles a non-polar rigid crystalline state while the parallel assembly is in agreement with a polar liquid crystal.

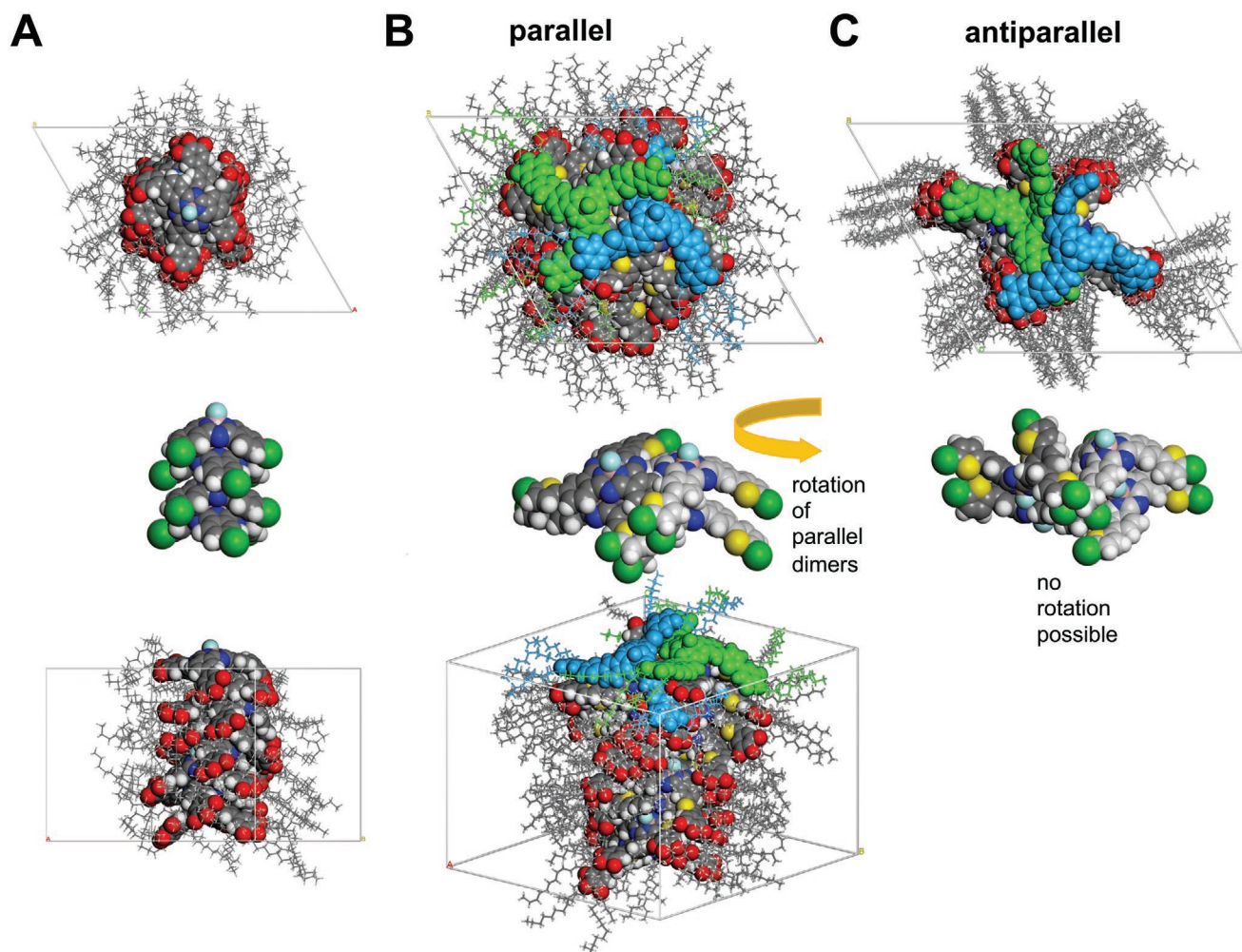


**Figure 6.** Columnar models of LC SubPcs **1a** and **1b**. A) Model of **1a** with staggered mesogens along the columnar axis. B) Parallel polar dimer model of **1b**. C) Antiparallel non-polar dimer model of **1b** leading to a more ordered arrangement.

## 6. Polar Properties

The polar nature of the new materials has been studied in more detail in filled LC cells of **1b** and **1c**. Upon cooling from the isotropic liquid to the LC state, a grainy texture is observed in the absence of an electric field. Application of a DC bias ( $5 \text{ V } \mu\text{m}^{-1}$ ) yielded a homeotropically aligned columnar phase as evidenced by a pseudo-isotropic texture and conoscopy (Figure 7). Temperature-dependent dielectric spectra of compound **1b** are shown in Figure 7C. Besides a mode in the range between 1–5 kHz, which disappears at low temperature, a strong low-frequency mode can be distinguished below 100 Hz. This mode shifts to even lower frequencies with decreasing temperature. This observation can be explained by increasing viscosity and consequently the shift of the relaxation rates to lower values. Application of a bias field results in a slight suppression of the mode (Figure 7D). The low frequency mode can be attributed to the extended polar correlations of the columns. Its presence even at  $180^\circ\text{C}$  suggests that those correlations already exist in the isotropic phase. Thus, polar aggregates are present in the isotropic phase which align in parallel under the action of an electric field. This is also corroborated by the observation of the

field-induced SHG signal in the isotropic phase. However, this signal disappears instantly after the external field is removed.

Preliminary experiments indicate the presence of a current increasing under UV-light (Figure 7E). This is analogous to the previous studies, in which photocurrents can be induced in polar LC phases without p-n junctions.<sup>[20]</sup> In the present case the absorption range and absorption intensity are increased over large portion of the visible spectral range, which should be of advantage for their application as photodetectors or photovoltaic materials. This high extinction coefficient results in small penetration lengths of the light and thus the absorption takes place mainly in a narrow layer close to the illuminated electrode. The slow increase of the photocurrent in Figure 7E can be attributed to the not optimal alignment of the LC featuring grainy walls capable of capturing charges and affecting the conductivity of the sample. Also the ionic impurities in the LC bulk contribute to the observed current. Annealing the sample from the isotropic phase in an external bias field of  $10 \text{ V}$  results in an increase in the photocurrent. However, a detailed analysis of the photocurrent requires further optimization of the device geometry and the measuring procedure which is currently in progress.

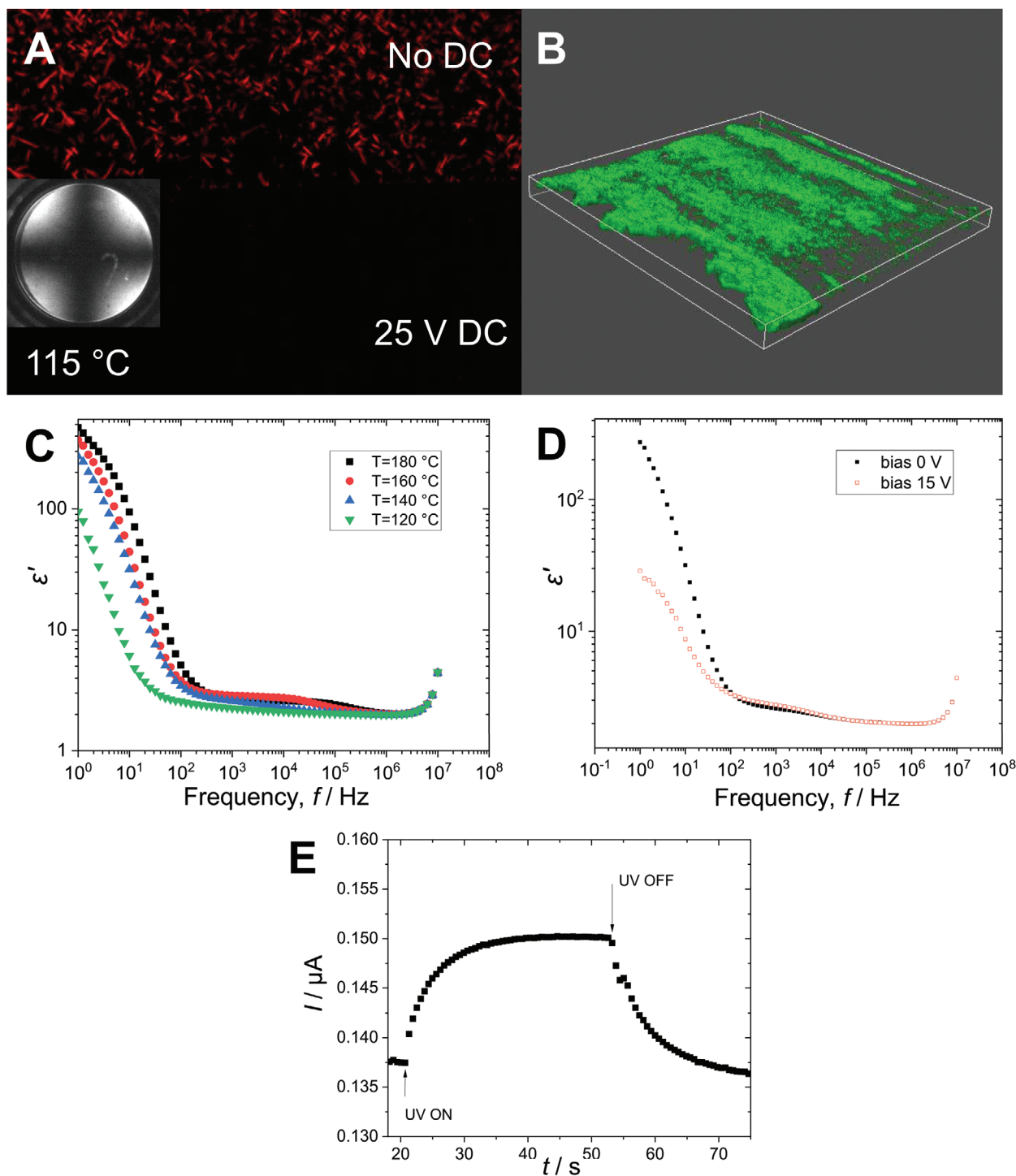


**Figure 7.** Polar Properties of **1b** and **1c**. A) Grainy texture of **1b** without E-field (top) and homeotropic texture with DC field (bottom); inset conoscopic image of a homeotropically aligned domain. B) Second harmonic generation (SHG) image of **1c** in a LC cell with interdigitated IPS electrodes. C) Dielectric spectra of **1b**. D) Dielectric spectra of **1b** with and without a bias voltage. E) Photoinduced changes of the current flowing through a 3  $\mu\text{m}$  LC cell of **1b** at 110  $^{\circ}\text{C}$  under illumination of UV light ( $360 \pm 12 \text{ nm}$ ,  $0.3 \text{ mW mm}^{-2}$ ) with an applied voltage of  $U = 10 \text{ V}$ .

## 7. Conclusion

In conclusion, we reported the synthesis of star-shaped SubPCs with oligothieryl arms. As a consequence of the additional conjugation the absorption range increases and the material

absorbs light up to 700 nm in thin films. All bowl (**1a**) and umbrella-shaped (**1b** and **1c**) mesogens form enantiotropic hexagonal columnar mesophases with clearing temperatures below 200  $^{\circ}\text{C}$ . The mesogens **1b** and **1c** generate polar dimers. This allows to align the columnar phases upon cooling to the

LC phase in the presence of an E-field. These phases possess polar domains as evidenced by a strong SHG signal and exhibit a photocurrent under UV light. Thus, additional charges are generated without the presence of a p-n junction. Further investigations are in progress, which will reveal the performance as function of the irradiation wavelengths and attached acceptor building blocks.

## 8. Experimental Section

**Synthesis and Characterization:** All commercial materials employed were used as received, without further purification.

Preparative recycling gel permeation chromatography was performed with the liquid chromatograph LC-20A (Shimadzu). The column set (PSS SDV 50 Å, 20-600 mm; PSS SDV 500 Å, 20-600 mm) was eluted with HPLC-grade CHCl<sub>3</sub> at a flow rate of 4.0 mL min<sup>-1</sup>.

The syntheses of the isomeric mixtures of compounds 1a–c were carried out using a convergent strategy, which is described in detail in the Supporting Information. A SubPc-based core building block was synthesized following known procedures and coupled with three equivalents of boronic acid derivatives or boronic acid esters of conjugated aromatic arm units in a threefold Suzuki cross coupling reaction according to a slightly adapted literature process in the final step.<sup>[29–30]</sup>

General preparation method for the final step: A solution of triiodosubphthalocyaninefluoride **2** (1 eq.) and cesium fluoride (9 eq.) in 20 mL dry THF as well as a solution of the boron acid (ester) compound (3.3 eq., **3**, **4** or **5**) in 15 mL dry THF were degassed in two different reaction flasks by flushing with nitrogen for 45 min. Both solutions were transferred into the reaction flask, Pd(dppf)Cl<sub>2</sub> was added in catalytic amounts to the mixture, and it was heated at reflux for 16 h. After cooling to RT, the reaction mixture was subjected to column chromatography (silica gel, eluent gradient: cyclohexane/CH<sub>2</sub>Cl<sub>2</sub> = 2:1 v/v → pure CH<sub>2</sub>Cl<sub>2</sub>). The products were isolated in 25–53% yield of the Suzuki reaction after further purification by GPC (eluent: CHCl<sub>3</sub>). Target compounds 1a–c were characterized by <sup>1</sup>H, <sup>13</sup>C NMR and mass spectrometry (MALDI-TOF).

NMR spectra were recorded on a Bruker-Daltonics Avance-400 spectrometer operating at 400 MHz (<sup>1</sup>H) or 101 MHz (<sup>13</sup>C) and on a Bruker-Daltonics Ascend-600 operating at 600 MHz (<sup>1</sup>H) or 151 MHz (<sup>13</sup>C), with the residual solvent signal used as the internal standard. The information for NMR characterization of new compounds and the assignment of <sup>1</sup>H- and <sup>13</sup>C-atom signals was drawn from <sup>1</sup>H, <sup>13</sup>C, DEPT135, COSY, HSQC and HMBC standard measurement methods. Mass spectra were recorded on a Bruker-Daltonics autoflex II (MALDI) and on a Bruker-Daltonics ultrafleXtreme (HRMS-MALDI). UV-Vis-absorption studies in solution (CHCl<sub>3</sub>) were performed on a JASCO V-770 spectrometer. An Edinburgh Instruments FLSP920 spectrometer equipped with a cooled red PMT detector from Hamamatsu (R13456-P) was used for emission measurements in solution. The instrument was equipped with double monochromators, operating in right angle geometry mode. A 450 W continuous xenon arc lamp (Xe900) was used as excitation source and was focused on the sample. Solutions of ≈10<sup>-7</sup> M concentration in CHCl<sub>3</sub> were prepared for all samples. Excitation wavelengths were chosen to match the local absorption maxima in the UV-Vis-spectra attributed to conjugated arm moieties. Slit widths of the instrument were optimized to reach a high intensity and good resolution for fluorescence spectrum of 1b, which was assumed to be the strongest emitter of the investigated series. Slit widths were kept constant for all subsequent measurements in order to allow for comparison of the fluorescence in the series of similar compounds.

**Analytical Data for 1a–c and 2:** SubPc **2**:<sup>[12]</sup> <sup>1</sup>H NMR (400 MHz, CDCl<sub>3</sub>): δ = 8.220, 8.222, 8.223, 8.226 (superimposed C<sub>1</sub>/C<sub>3</sub>, dd, <sup>3</sup>J = 8.33 Hz, <sup>4</sup>J = 1.48 Hz, 3 H, arom. H, H-3, H-3', H-3'', H-3'''), 8.551, 8.556, 8.558, 8.562 (superimposed C<sub>1</sub>/C<sub>3</sub>, dd, <sup>3</sup>J = 8.33 Hz, <sup>5</sup>J = 0.60 Hz, 3 H, arom.

H, H-4, H-4', H-4'', H-4'''), 9.209, 9.211, 9.212, 9.214 (superimposed C<sub>1</sub>/C<sub>3</sub>, dd, <sup>3</sup>J = 1.48 Hz, <sup>5</sup>J = 0.60 Hz, 3 H, arom. H, H-2, H-2', H-2'', H-2''') ppm. The coupling constants were determined by the simulation with the program MestRe-C 2.3a (see Figure 2 and Figure S3: Supporting Information).

**SubPh 1a:** <sup>1</sup>H NMR (400 MHz, CDCl<sub>3</sub>): δ = 0.84–0.90 (27 H, –CH<sub>3</sub>), 1.21–1.43 (144 H, –CH<sub>2</sub>–), 1.49–1.60 (18 H, –CH<sub>2</sub>–), 1.77–1.93 (18 H, –CH<sub>2</sub>–), 4.02–4.18 (18 H, –OCH<sub>2</sub>–), 7.02–7.05 (superimposed C<sub>1</sub>/C<sub>3</sub>, 6 H, arom. H, H-3, H-3'), 8.14 (superimposed C<sub>1</sub>/C<sub>3</sub>, d, 3 H, <sup>3</sup>J = 8.3 Hz, arom. H, H-7), 8.90 (superimposed C<sub>1</sub>/C<sub>3</sub>, d, 3 H, <sup>3</sup>J = 8.3 Hz, arom. H, H-8), 9.05 (superimposed C<sub>1</sub>/C<sub>3</sub>, bs, 3 H, arom. H, H-6) ppm. <sup>13</sup>C NMR (151 MHz, CDCl<sub>3</sub>): δ = 14.3 (CH<sub>3</sub>), 22.8, 26.3, 29.6, 30.7, 32.2 (CH<sub>2</sub>), 69.7, 73.8 (OCH<sub>2</sub>), 106.6 (C<sub>q</sub>, C-3, C-3'), 120.6 (aromat. CH, C-6), 122.3 (aromat. CH, C-8), 129.3 (aromat. CH, C-7), 129.8 (C<sub>q</sub>, C-4), 138.9 (C<sub>q</sub>, C-1), 143.6 (C<sub>q</sub>, C-5), 153.8 (C<sub>q</sub>, C-2, C-2') ppm. It was not possible to detect the signals for the quaternary carbon atoms of the subphthalocyanine core as their intensity was too low due to the different chemical shifts for C<sub>1</sub>/C<sub>3</sub> isomers. HR-MALDI-TOF calculated for C<sub>150</sub>H<sub>239</sub>BFN<sub>6</sub>O<sub>9</sub>: [M<sup>+</sup>] = m/z (monoisotopic): 2298.8524, found: 2298.8500, error: 1.06 ppm.

UV-vis (CHCl<sub>3</sub>): λ<sub>max</sub>(ε) = 286 (4950), 583 nm (5240).

**SubPh 1b:** <sup>1</sup>H NMR (600 MHz, CD<sub>2</sub>Cl<sub>2</sub>): δ = 0.85–0.91 (27 H, –CH<sub>3</sub>), 1.24–1.42 (144 H, –CH<sub>2</sub>–), 1.44–1.56 (18 H, –CH<sub>2</sub>–), 1.70–1.88 (18 H, –CH<sub>2</sub>–), 3.96 (t, 6 H, <sup>3</sup>J = 6.6 Hz, –OCH<sub>2</sub>–), 4.04 (t, 12 H, <sup>3</sup>J = 6.6 Hz, –OCH<sub>2</sub>–), 6.82 (superimposed C<sub>1</sub>/C<sub>3</sub>, s, bs, 6 H, arom. H, H-3, H-3'), 7.22 (m, 3 H, arom. H, H-6), 7.29 (m, 6 H, arom. H, H-7, H-10), 7.63 (d, 3 H, <sup>3</sup>J = 3.8 Hz, arom. H, H-11), 8.14–8.18 (superimposed C<sub>1</sub>/C<sub>3</sub>, 3 H, arom. H, H-15), 8.77–8.82 (superimposed C<sub>1</sub>/C<sub>3</sub>, 3 H, arom. H, H-16), 9.05 (superimposed C<sub>1</sub>/C<sub>3</sub>, bs, 3 H, arom. H, H-14) ppm. <sup>13</sup>C NMR (151 MHz, CD<sub>2</sub>Cl<sub>2</sub>): δ = 13.9 (CH<sub>3</sub>), 22.7, 26.2, 29.5, 29.7, 30.4 (CH<sub>2</sub>), 69.1, 73.5 (OCH<sub>2</sub>), 118.3 (aromat. CH, C-14), 122.6 (aromat. CH, C-16), 123.6 (aromat. CH, C-6), 125.0 (aromat. CH, C-7), 125.0 (aromat. CH, C-10), 125.7 (aromat. CH, C-3, C-3'), 125.7 (aromat. CH, C-11), 127.1 (aromat. CH, C-15), 129.0 (C<sub>q</sub>, C-4), 135.8 (C<sub>q</sub>, C-8), 136.0 (C<sub>q</sub>, C-12), 138.2 (C<sub>q</sub>, C-1), 138.5 (C<sub>q</sub>, C-9), 142.0 (C<sub>q</sub>, C-13), 144.2 (C<sub>q</sub>, C-5), 153.5 (C<sub>q</sub>, C-2, C-2') ppm. It was not possible to detect signals for the quaternary carbon atoms of the SubPh core as their intensities were too low due to the different chemical shifts of signals of C<sub>1</sub>/C<sub>3</sub> isomers. HR-MALDI-TOF calculated for C<sub>174</sub>H<sub>252</sub>BFN<sub>6</sub>O<sub>9</sub>S<sub>6</sub>: [M<sup>+</sup>] = m/z (monoisotopic): 2790.7769, found: 2790.7763, error: 0.22 ppm.

UV-vis (CHCl<sub>3</sub>): λ<sub>max</sub>(ε) = 333 (6560), 404 (4620), 606 nm (9920).

**SubPh 1c:** <sup>1</sup>H NMR (600 MHz, CD<sub>2</sub>Cl<sub>2</sub>): δ = 0.85–0.91 (27 H, –CH<sub>3</sub>), 1.24–1.42 (144 H, –CH<sub>2</sub>–), 1.44–1.56 (18 H, –CH<sub>2</sub>–), 1.70–1.88 (18 H, –CH<sub>2</sub>–), 3.96 (t, 6 H, <sup>3</sup>J = 6.6 Hz, –OCH<sub>2</sub>–), 4.04 (t, 12 H, <sup>3</sup>J = 6.6 Hz, –OCH<sub>2</sub>–), 6.82 (superimposed C<sub>1</sub>/C<sub>3</sub>, s, bs, 6 H, arom. H, H-3, H-3'), 7.22 (m, 3 H, arom. H, H-6), 7.29 (m, 6 H, arom. H, H-7, H-10), 7.63 (d, 3 H, <sup>3</sup>J = 3.8 Hz, arom. H, H-11), 8.14–8.18 (superimposed C<sub>1</sub>/C<sub>3</sub>, 3 H, arom. H, H-15), 8.77–8.82 (superimposed C<sub>1</sub>/C<sub>3</sub>, 3 H, arom. H, H-16), 9.05 (superimposed C<sub>1</sub>/C<sub>3</sub>, bs, 3 H, arom. H, H-14) ppm. <sup>13</sup>C NMR (151 MHz, CD<sub>2</sub>Cl<sub>2</sub>): δ = 13.9 (CH<sub>3</sub>), 22.7, 26.2, 29.5, 29.7, 30.4 (CH<sub>2</sub>), 69.1, 73.5 (OCH<sub>2</sub>), 118.3 (aromat. CH, C-14), 122.6 (aromat. CH, C-16), 123.6 (aromat. CH, C-6), 125.0 (aromat. CH, C-7), 125.0 (aromat. CH, C-10), 125.7 (aromat. CH, C-3, C-3'), 125.7 (aromat. CH, C-11), 127.1 (aromat. CH, C-15), 129.0 (C<sub>q</sub>, C-4), 135.8 (C<sub>q</sub>, C-8), 136.0 (C<sub>q</sub>, C-12), 138.2 (C<sub>q</sub>, C-1), 138.5 (C<sub>q</sub>, C-9), 142.0 (C<sub>q</sub>, C-13), 144.2 (C<sub>q</sub>, C-5), 153.5 (C<sub>q</sub>, C-2, C-2') ppm. It was not possible to detect <sup>13</sup>C NMR signals for the quaternary carbon atoms of the subphthalocyanine core as their intensity was too low presumably due to the different chemical shifts of signals of C<sub>1</sub>/C<sub>3</sub> isomers. NMR data indicates that the compound is a mixture of both C<sub>3</sub>/C<sub>1</sub> isomers in the ratio 1:3. HR-MALDI-TOF calculated for C<sub>174</sub>H<sub>252</sub>BFN<sub>6</sub>O<sub>9</sub>S<sub>6</sub>: [M<sup>+</sup>] = m/z (monoisotopic): 2790.7769, found: 2790.7763, error: 0.22 ppm.

UV-vis (CHCl<sub>3</sub>): λ<sub>max</sub>(ε) = 366 (6300), 418 (5770), 612 nm (8510).

**Investigation of Thermotropic Properties:** The studies of optical textures of the mesophases as well as absorption and emission measurements in thin film were realized with a Nikon Eclipse LV100Pol optical polarizing microscope equipped with a Linkam LTS420 heating stage, a Linkam T95-HS system controller and a StellarNet BLACK-Comet CXR-100



USB Spectrometer. A Nikon C-LHGFI HG lamp was used as excitation light source for solid state fluorescence measurements in the same experimental setup. The temperature dependent SAXS, MAXS and WAXS X-ray investigations were performed on a Bruker Nanostar (Detector Vantec2000, Microfocus copper anode X-ray tube Incoatec). The aligned fibers were transferred to Mark capillaries, which were sealed and glued into the metal sample holder. The XRS heating system was calibrated by liquid crystal standard compounds. The XRS data was evaluated by the program *datasqueeze* using silver behenate as a calibration standard.

The DSC measurements were performed on a PerkinElmer DSC 8500 equipped with cryofill cooling system and Pt/Ir ovens. The samples were sealed in TA hermetic pans and lids. All measurements were performed with a rate of 10 K min<sup>-1</sup> and were evaluated with *Pyrus* Software for Windows.

**Study of Polar Properties:** For dielectric spectroscopy measurements, 5 μm thick cells with gold electrodes have been used. The material was introduced into the cells using capillary suction in its isotropic state. The dielectric measurements were made using Solatron 1260A impedance analyzer (Ametek, USA) in the frequency range from 10 Hz to 10 MHz. Generation of the optical second harmonic (SHG) was measured using a confocal microscope TCS SP8-Leica. A tunable IR laser ( $\lambda = 880$  nm) was used as a fundamental light. As a liquid crystal device, 6 μm cells were used with interdigitated IPS electrodes. An electric field was applied by an arbitrary-wave generator (TTi) with a field amplitude varying from 0 to 120 V at 20 Hz. Fundamental light was incident normally to the planarly LC cells. The SHG signal was collected by a photomultiplier tube at 440 nm.

## Supporting Information

Supporting Information is available from the Wiley Online Library or from the author.

## Acknowledgements

M.L. and A.E. are grateful for the financial support by the German Science Foundation (DFG) via LE 1571/11-1 and ER 467/17-1.

Open access funding enabled and organized by Projekt DEAL.

## Conflict of Interest

The authors declare no conflict of interest.

## Data Availability Statement

The data that supports the findings of this study are available in the supplementary material of this article.

## Keywords

columnar phases, ferroelectrics, liquid crystal alignment, organic semiconductors, subphthalocyanine

Received: May 4, 2021

Revised: June 18, 2021

Published online: July 4, 2021

- [1] R. B. Meyer, L. Liébert, L. Strzelecki, P. Keller, *J. Phys. (France)* **1975**, 36, L.
- [2] S. T. Lagerwall, in *Handbook of Liquid Crystals*, Vol. 4, 2nd ed. (Eds: J. W. Goodby, P. J. Collings, T. Kato, C. Tschierske, H. Gleeson, P. Raynes), Wiley-VCH, Weinheim, Germany **2014**, pp. 129–386.
- [3] L. Vicari, *Optical Applications of Liquid Crystals*, Institute of Physics Publishing, Bristol and Philadelphia **2003**.
- [4] T. Niori, F. Sekine, J. Watanabe, T. Furukawa, H. Takezoe, *J. Mater. Chem.* **1996**, 6, 1231.
- [5] D. Miyajima, F. Araoka, H. Takezoe, J. Kim, K. Kato, M. Takata, T. Aida, *Science* **2012**, 336, 209.
- [6] E. Dalcanale, A. du Vosel, A. M. Levelut, J. Malh ete, *Liq. Cryst.* **1991**, 10, 185.
- [7] R. Poupko, Z. Luz, N. Spielberg, H. Zimmermann, *J. Am. Chem. Soc.* **1989**, 111, 6094.
- [8] H. Bock, W. Helfrich, *Liq. Cryst.* **1992**, 12, 697.
- [9] G. Scherowsky, X. H. Chen, *J. Mater. Chem.* **1995**, 5, 417.
- [10] J. Barber , R. Iglesias, J. L. Serrano, T. Sierra, M. R. de la Fuente, B. Palacios, M. A. P rez-Jubindo, J. T. V zquez, *J. Am. Chem. Soc.* **1998**, 120, 2908.
- [11] S. H. Kang, Y.-S. Kang, W.-C. Zin, G. Olbrechts, K. Wostyn, K. Clays, A. Persoons, K. Kim, *Chem. Commun.* **1999**, 1661.
- [12] J. Guilleme, J. Arag , E. Ort , E. Caverro, T. Sierra, J. Ortega, C. L. Folcia, J. Etxebarria, D. Gonz lez-Rodr guez, T. Torres, *J. Mater. Chem. C* **2015**, 3, 985.
- [13] J. Guilleme, E. Caverro, T. Sierra, J. Ortega, C. L. Folcia, J. Etxebarria, T. Torres, D. Gonz lez-Rodr guez, *Adv. Mater.* **2015**, 27, 4280.
- [14] Y. Ren, A. M. Hiszpanski, Y.-L. Loo, *Chem. Mater.* **2015**, 27, 4008.
- [15] C. G. Claessens, D. Gonz lez-Rodr guez, M. S. Rodr guez-Morgade, A. Medina, T. Torres, *Chem. Rev.* **2014**, 114, 2192.
- [16] C. E. Mauldin, C. Piliago, D. Poulsen, D. A. Unruh, C. Woo, B. Ma, J. L. Mynar, J. M. J. Fr chet, *ACS Appl. Mater. Interfaces* **2010**, 2, 2833.
- [17] M. J. Mayoral, T. Torres, D. Gonz lez-Rodr guez, *J. Porphyrins Phthalocyanines* **2020**, 24, 33.
- [18] Y. Funatsu, A. Sonoda, M. Funahashi, *J. Mater. Chem. C* **2015**, 3, 1982.
- [19] A. Seki, Y. Funatsu, M. Funahashi, *Phys. Chem. Chem. Phys.* **2017**, 19, 16446.
- [20] C. Zhang, K. Nakano, M. Nakamura, F. Araoka, K. Tajima, D. Miyajima, *J. Am. Chem. Soc.* **2020**, 142, 3326.
- [21] K. T. Butler, J. M. Frost, A. Walsh, *Energy Environ. Sci.* **2015**, 8, 838.
- [22] M. Lehmann, M. Dechant, M. Holzappel, A. Schmiedel, C. Lambert, *Angew. Chem., Int. Ed.* **2019**, 58, 3610.
- [23] M. Lehmann, M. Dechant, M. Lambov, T. Ghosh, *Acc. Chem. Res.* **2019**, 52, 1653.
- [24] M. Dechant, M. Lehmann, G. Uzurano, A. Fujii, M. Ozaki, *J. Mater. Chem. C* **2021**, 9, 5689.
- [25] J. Guilleme, M. J. Mayoral, J. Calbo, J. Arag , P. M. Viruela, E. Ort , T. Torres, D. Gonz lez-Rodr guez, *Angew. Chem., Int. Ed.* **2015**, 54, 2543.
- [26] C. G. Claessens, T. Torres, *Tetrahedron Lett.* **2000**, 41, 6361.
- [27] J. Kesters, P. Verstappen, M. Kelchtermans, L. Lutsen, D. Vanderzande, W. Maes, *Adv. Energy Mater.* **2015**, 5, 1500218.
- [28] E. Bukuroshi, J. Vestfrid, Z. Gross, T. P. Bender, *New J. Chem.* **2019**, 43, 16730.
- [29] M. V. Fulford, D. Jaidka, A. S. Paton, G. E. Morse, E. R. Brisson, A. J. Lough, T. B. Bender, *J. Chem. Eng. Data* **2009**, 57, 2756.
- [30] D. Gonz lez-Rodr guez, T. Torres, *Eur. J. Org. Chem.* **2009**, 2009, 1871.